

# Synergistic effects of electrolytic manganese residue-red mud-carbide slag on the road base strength and durability properties

Yuliang Zhang<sup>a</sup>, Xiaoming Liu<sup>a,\*</sup>, Yingtang Xu<sup>a</sup>, Binwen Tang<sup>a</sup>, Yaguang Wang<sup>a</sup>, Emile Mukiza<sup>b</sup>

<sup>a</sup> School of Metallurgical and Ecological Engineering, University of Science and Technology Beijing, 100083, China

<sup>b</sup> School of Energy and Environmental Engineering, University of Science and Technology Beijing, 100083, China

## HIGHLIGHTS

- Synergistic effect of EMR, RM and CS was proposed.
- Excellent mechanical and durability performance obtained under synergistic action.
- The EMR-RM-CS hydrated paste has well polymerized [SiO<sub>4</sub>] structure.
- Al<sup>IV</sup> and Al<sup>VI</sup> both exist in the synergistic system.
- Heavy metals can be well solidified by the road base material.

## ARTICLE INFO

### Article history:

Received 4 April 2019

Received in revised form 21 May 2019

Accepted 3 June 2019

Available online 11 June 2019

### Keywords:

Electrolytic manganese residue

Red mud

Carbide slag

Road base material

Synergy

## ABSTRACT

The present study was designed to prepare the road base material by using electrolytic manganese residue (EMR), red mud (RM) and carbide slag (CS) as main raw materials. The mix was optimized and mechanical properties, durability, strength formation mechanism and environmental behavior were investigated. X-ray diffraction (XRD), Mercury intrusion porosimetry (MIP), <sup>29</sup>Si and <sup>27</sup>Al magic-angle spinning (MAS) nuclear magnetic resonance (NMR) and electron probe microanalysis method (EPMA) were used for microstructure characterization. The results show that after curing for 7 days, the EMR-RM-CS exhibited the highest unconfined compressive strength (UCS), showed the best durability, the best pore diameter distribution and critical pore size. Hydration characteristics reveal that C-A-S-H gel and AFt are generated in EMR-RM-CS, which is positive to the form of UCS and durability. <sup>29</sup>Si analysis demonstrates that the synergy of EMR, RM and CS has the best polymerized structure. Al in the hydrated pastes exists in the form of Al<sup>IV</sup> and Al<sup>VI</sup>, and one part of the dominant Al<sup>IV</sup> is activated and another one is converted to Al<sup>VI</sup>. The leaching results meet the Chinese groundwater standards which indicate that EMR-RM-CS system can well solidify the heavy metals. The road base material prepared by EMR not only consumes a significant quantity of solid wastes but also provides a new idea for the synergistic utilization of solid wastes.

© 2019 Elsevier Ltd. All rights reserved.

## 1. Introduction

Electrolytic manganese residue (EMR), red mud (RM) and carbide slag (CS) are three kinds of solid waste which are largely produced and difficult to recycle. EMR is a potentially harmful industrial solid waste, its major hazardous substances are heavy metals and ammonia nitrogen, which are harmful to the environment [1]. China is the largest producer of electrolytic manganese in the world with about 1.66Mt produced in 2018 [2]. Every ton

of manganese produced generates 10–12 tons of EMR [3], implying that more than 15.5Mt EMR are produced annually. Red mud is the powder solid residue of bauxite after strong alkali leaching of alumina. For every ton of alumina produced will bring 1.0–1.8 tons of red mud [4,5]. Red mud contains a large number of strong alkaline chemicals with a pH value of more than 12 [6], and the main harmful element in RM is sodium. Carbide slag is an industrial waste produced by calcium carbide hydrolysis to prepare C<sub>2</sub>H<sub>2</sub> gas, PVC, etc. [7,8]. The carbide slag had been identified as an industrial solid waste, which is difficult to be recycled. [9,10]. Moreover, it is also a highly alkaline solid slag. At present, the disposal methods of these residues are open-air accumulation or landfill which may cause the harmful substances in the three kinds of waste residues to infil-

\* Corresponding author at: Room 313, School of Metallurgical and Ecological Engineering, University of Science and Technology Beijing, Beijing 100083, China.  
E-mail address: [liuxm@ustb.edu.cn](mailto:liuxm@ustb.edu.cn) (X. Liu).

trate into the soil or flow into rivers with rainwater, thereby causing harm to the soil and groundwater, and then endanger the ecological environment. Therefore, the comprehensive utilization of solid waste is particularly important.

Nowadays, the utilization of the three kinds of waste residues is mainly in the preparation of building materials. EMR is used in autoclaved bricks [1], ecological cement [11], geopolymer [12]; RM is used to replace clay for non-burned brick [13], road materials [14] and cementitious material [15]; while CS could be used as an alternative for limestone in cement production, xonotlite [16,17]. These studies provide a practical and theoretical basis for the utilization of the three solid wastes. Liu [18] investigated the composite activator of industrial solid waste carbide slag and desulphurization gypsum; it was found that they stimulate the activity of Bayer red mud and make it exhibit hydraulically cementitious properties. The compressive strength of 28 days can reach more than 7 MPa. Chen [19] studied on activation of slag by EMR and RM composite, and it was found that when the mass ratio of steel slag, RM and EMR was 3:1:2, the activity index of steel slag increased from 46% to 82% in 7 days and from 61% to 82% in 28 days. There have been many reports on the individual utilization technologies of EMR, RM and CS, synergic use of them need to be further studied. It is necessary to investigate the synergistic effect to realize large-scale utilization of solid waste.

This paper innovative proposals on the utilization of EMR, RM and CS as main raw materials to prepare road base material, mainly focuses on the unconfined compressive strength (UCS), durability properties and its synergistic mechanism. In addition, use different detection methods such as X-ray diffraction (XRD), Mercury intrusion porosimetry (MIP), <sup>29</sup>Si and <sup>27</sup>Al magic-angle spinning (MAS) nuclear magnetic resonance (NMR) and electron probe microanalysis method (EPMA) to obtain the synergistic mechanism of EMR-RM-CS system. The research results provide a basis for the synergistic utilization of various solid wastes, conducive to reduce the pollution of EMR, RM and CS to the environment, demonstrate significant environmental and economic benefits.

## 2. Experiment

### 2.1. Materials

The road base material including EMR, RM, CS, aggregate and a small amount of admixture and grade 42.5 ordinary Portland cement (OPC). EMR used in this research was obtained from Guizhou electrolytic manganese plant by the hydrometallurgy process, and its pH value is 6.0. RM was from Guizhou alumina plant; the smelting method is the Bayer process; and its pH value is 10.9. CS was obtained from Guizhou acetylene plant; and its pH value is 11.2. Their chemical composition was analyzed by X-ray fluorescence (XRF) and presented in Table 1. The mineralogical phases of raw materials were analyzed by XRD, as shown in Fig. 1. Combining XRD and XRF results, it can be seen that the main mineralogical phases in EMR are quartz (SiO<sub>2</sub>) and gypsum (CaSO<sub>4</sub>·H<sub>2</sub>O), its SO<sub>4</sub><sup>2-</sup> content is high, which can be used to form Aft in an alkali environment. The aluminous minerals in RM are high, which can provide enough Al to the system. The main substance in CS is Ca(OH)<sub>2</sub>,

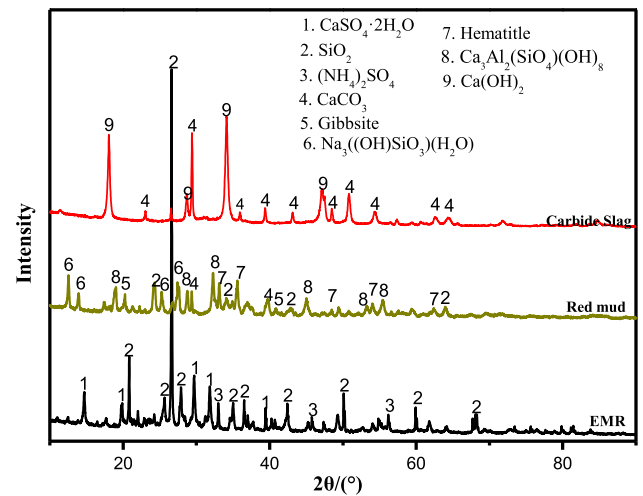


Fig. 1. Mineralogical phases of raw materials.

which can supplement enough calcium and OH<sup>-</sup> to provide a high alkaline environment for promoting hydration reaction. It can be inferred that the Al-O, Si-O and Ca-O content in the system can be stimulated by OH<sup>-</sup>, partially combine with SO<sub>4</sub><sup>2-</sup> to generate hydraulic substances that make the system having hydraulically cementitious properties.

### 2.2. Experimental procedures

Different proportions of raw materials were designed and the compressive strength was tested to find a suitable proportion of road base material. The designed proportions are presented in Table 2. The mix design is based on the Chinese standard “Technical Specifications for Construction of Highway Roadbases”. It can be seen that the ratio of EMR: RM: CS are 6:0:1, 6:2:1 and 3:1:0, respectively. This study mainly focuses on the mechanical properties and synergistic mechanism of the three ratios.

According to Chinese standard T0843-2009, specimens of 50 × 50 mm were prepared according to the proportions listed in Table 2. Raw materials were mixed to uniformity and water was added based on the optimum water content to achieve maximum dry density. The mixture was stored in an airtight to prevent the loss of water. Waterproof bag for 18–24 h prior to making the test specimens to get a uniform distribution of the moisture throughout the whole mixture. The less water added and the more quality of the mixture, the moisture can not be distributed evenly in the mixture very soon. After 18–24 h, the moisture will be distributed more evenly in the mixture, which makes the mixture reach the optimum moisture content and reduces the strength error.

Table 2  
Mix design of road base material (mass fraction%).

Mix name	EMR	RM	CS	Admixture	Aggregate	Extra cement
1	30	–	5	5	60	3
2	30	10	5	5	50	3
3	30	10	–	5	55	3

Table 1  
Chemical composition of raw materials.

Constituents	SiO <sub>2</sub>	SO <sub>3</sub>	Al <sub>2</sub> O <sub>3</sub>	CaO	Fe <sub>2</sub> O <sub>3</sub>	MnO	K <sub>2</sub> O	MgO	Na <sub>2</sub> O	TiO <sub>2</sub>	LOI
EMR	31.38	18.58	10.71	9.45	7.53	4.82	3.4	1.61	0.77	0.57	10.02
RM	18.71	1.73	22.72	13.96	20.48	–	2.08	0.71	8.61	3.34	7.02
CS	4.09	1.26	2.18	83.69	0.72	–	–	0.89	–	0.15	7.01

The specimens were moulded into a  $\Phi 50 \times 50$  mm cylinder. The forming pressure was 20 MPa and the degree of compaction was 98%. The pressure was maintained for 2 min and then the sample was demoulded, sealed in airproof plastic bags and cured in a cabinet at  $20 \pm 2$  °C and 95% humidity until the appropriate age. After completion of the curing process, specimens were soaked for 24 h before compressive strength testing. The best proportion of road base material was subjected to further testing for long-term strength evaluation, mechanism analysis, and environmentally friendly performance. To investigate the hydration characteristics of the road base material, the pastes were prepared without aggregates using water to solid proportion of 0.5. The resulting pastes were moulded in  $20 \text{ mm} \times 20 \text{ mm} \times 20 \text{ mm}$  frame and cured at  $20 \pm 2$  °C and 95% humidity. The specimens for microstructure analysis were immersed in ethanol for 48 h to stop the hydration reaction and then dried at 60 °C for 24 h.

### 2.3. Test conditions

1. The maximum dry density and the optimum moisture content were obtained by the compaction test according to T0804-1994 (similar to ASTM D698-78 [20]) and the potential expansion tests, which are regulated by the ASTM D1883 standard [21]. Measuring the expansion performance of compacted materials by expansion sensor. The results show that the expansion of the EMR-RM-CS road base material is less than 1%. Under the synergistic action of raw materials, the expansion of road base material will not appear. The UCS test was conducted as per the testing method T0805-1994 (similar to ASTM D2850-87 [22]) for materials stabilized with inorganic binders for highway engineering (Ministry of Transport of the People's Republic of China, 2009).
2. The synergistic mechanism was tested through the micro-detection method: The phase analysis by XRD was done using Bruker D8 ADVANCE X-ray diffractometer with CuK $\alpha$  radiation, voltage 40 kV, current 200 mA and  $2\theta$  scanning, ranging from  $10^\circ$  to  $90^\circ$ . MAS NMR spectroscopy was measured by a BRUKER-AM300 spectrometer (Germany), 59.62 MHz for the  $^{29}\text{Si}$  resonance frequency and 78.20 MHz for the  $^{27}\text{Al}$  resonance frequency. SEM was carried out by means of Hitachi SU8020 scanning electron microscope. The microscale elemental distribution mapping was done by electron probe microanalysis method (EPMA) using EPMA-1720H, Shimadzu, Japan. The pore structure of samples tested by Autopore IV 9510 Mercury intrusion porosimetry (MIP).
3. For Backscattered Electron (BSE) test, the hydrated pastes were cut into 5–10 mm thin sections and immersed in isopropanol, after removing the free water, the slices were saturated with resin to support the microstructures [23,24], the detailed polishing method has been discussed by Hu and Li [25,26,27]. Then polished with sandpaper of different sizes to obtain a smooth surface. Finally, the samples were sprayed with metal for subsequent testing under electron microscopy [28].

## 3. Results

### 3.1. The compaction test

The three main raw materials that make the road base have quite different densities. Thus, the ratio of mixture significantly affects the dry density. Fig. 2 shows the maximum dry density and the optimum water content of road base materials in different proportions. Relevant information was shown in Table 3.

The 7 d UCS of different ratio was illustrated in Fig. 3, it can be seen that the peak value of strength is achieved when the ratio of EMR:RM:CS is 6:2:1, and it exceeds the standard of highway road

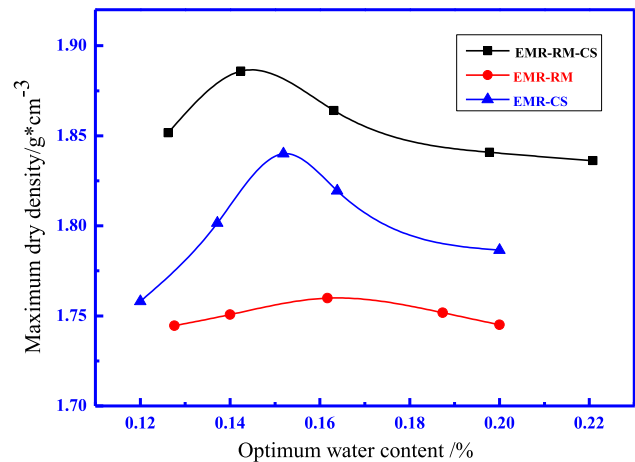


Fig. 2. Dry density and water content of mixture materials.

**Table 3**  
Relevant information of road base materials.

Road base materials	Ratio	pH	Maximum dry density (g/cm <sup>3</sup> )	Optimal water content (%)
EMR-RM-CS	6: 2: 1,	10.1	1.89	14.2
EMR-RM	3: 1: 0	8.6	1.84	15.1
EMR-CS	6: 0: 1	7.9	1.75	16.2

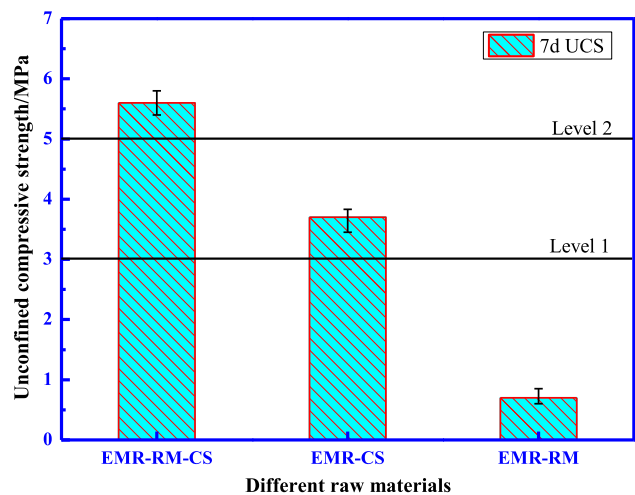


Fig. 3. The UCS of different ratios after curing for 7 days.

base in China (3–5 MPa). This is mainly due to the synergy of the three raw materials. The strength of the EMR-RM and EMR-CS are lower, 0.7 MPa and 3.7 MPa, respectively. The Ca(OH)<sub>2</sub> was used to replace carbide slag to prepare road base material also be evaluated. The results show that after curing for 7 days, the UCS of EMR-Ca(OH)<sub>2</sub> and EMR-Ca(OH)<sub>2</sub>-RM were 4.3 MPa and 5.7 MPa, respectively. The performance is slightly better than mixed carbide slag (3.7 MPa and 5.6 MPa). So, if there is not enough carbide slag, Ca(OH)<sub>2</sub> can be used to achieve the same effect.

The strength development of the road base material in different proportion is shown in Fig. 4. As shown in Fig. 4, the UCS of the three proportion is increased with the increase of curing age, especially the UCS of EMR-RM-CS increases more sharply than the others; its 28d strength can reach up to 8.4 MPa, and the strength of EMR-RM and EMR-CS are 5.2 MPa, 3.1 MPa respectively. Thus, the strength of the road base materials developed sharply following the curing age.

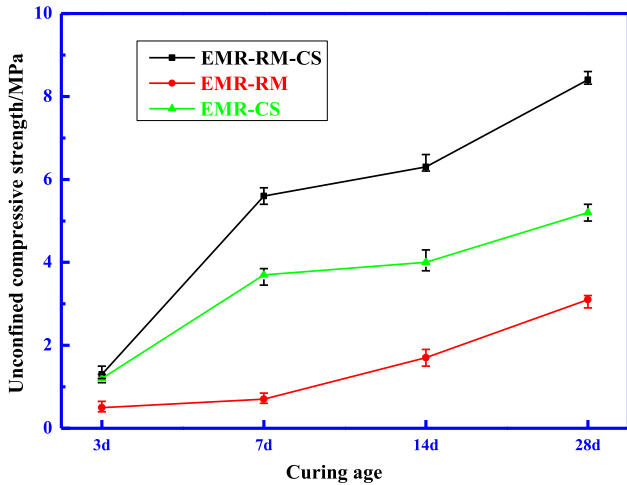


Fig. 4. Variation of UCS with curing time.

3.2. Durability properties

Road base materials will be used in different areas. Therefore, besides the basic physical and mechanical properties of road base, it is also necessary to study the frost resistance and wetting-drying resistance of road base materials [29].

3.2.1. Freezing-thawing test

The three different proportion samples were cured for 28 days as required by the standards prior to freeze-thaw cycles test. One cycle consists of freezing specimens at the temperature of -18 °C for 16 h, and then thawed in water at 20 °C for 8 h. The water is at least 20 mm higher than the surface of the specimens [30]. After each cycle, the specimens are wiped out and weighed. After completing 5 cycles, the UCS test was carried out on frozen specimens. The results are shown in Fig. 5. The frost resistance index (BDR) was calculated as follows:

$$BDR = \frac{R_{DC}}{R_C} \times 100\% \quad (1)$$

- BDR = The change of UCS after freeze-thaw cycles (%)
- $R_{DC}$  = The UCS of specimens after freeze-thaw cycles
- $R_C$  = The UCS of non-frozen specimens

It can be seen from Fig. 5 that after 5 cycles the strength are 7.1 MPa, 2.3 MPa and 0.9 MPa respectively, the UCS of EMR-CS-RM changed a little, still exceeding China’s highway standards. But the strength of EMR-RM and EMR-CS decreased greatly. The

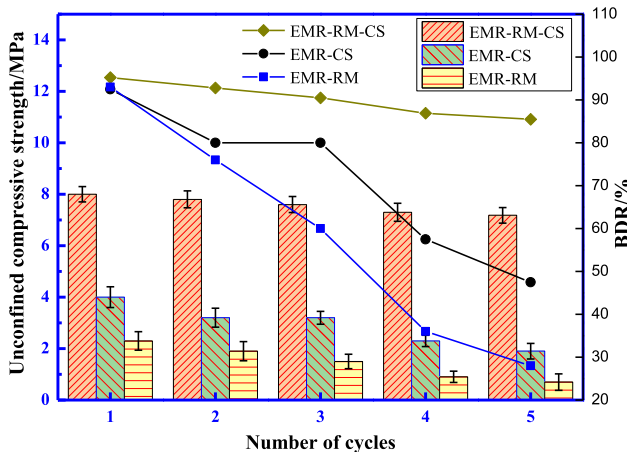


Fig. 5. UCS and BDR of each circle.

BDR are 85.47%, 47.5% and 28% respectively. The BDR value of traditional cement stabilized macadam road base material after five freeze-thaw cycles are about 80%. It can be concluded that the synergistic effect of the EMR, RM and CS road base materials have good frost resistance. The reason is that the three materials synergize to form hydration products with better frost resistance, which can better resist low temperature.

3.2.2. Wetting-drying cycle test

Wet-dry cycle is an important test of the durability of road base material [31]. The road base material often encounters the alternating state of dry and wet due to the influence of climate conditions. The moisture content in the material is constantly changing while it is known that water has a great influence on the strength and stability of the high-grade road base. Thus, this change will cause the expansion and contraction of the materials in the road base.

The 28-day cured specimens were used for wet-dry cycles test. One cycle consisted of soaking specimens in water at room temperature for 5 h, then dry them at 70 °C for 42 h, and then dry them in air for 1 h (48 h). After attaining the desired number of cycles, specimens were soaked for 2 h and dried for at least 2 h before testing the UCS [32]. Figs. 6 and 7 show the UCS and weight loss respectively after 1, 3, 6, 9, 15, 18 and 20 cycles.

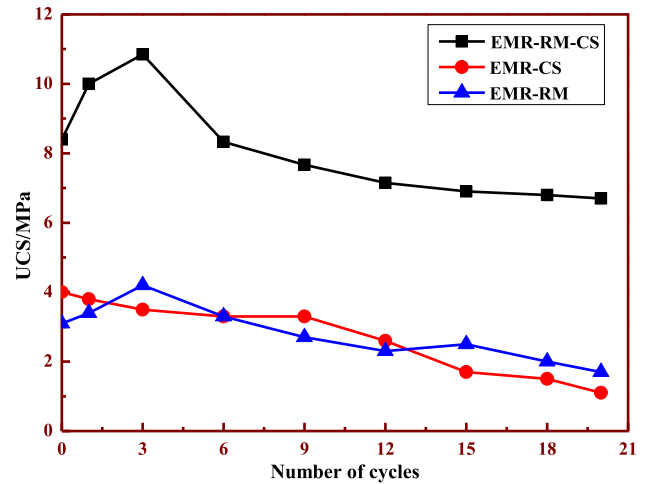


Fig. 6. UCS of the road base materials varying with the number of wetting-drying cycles.

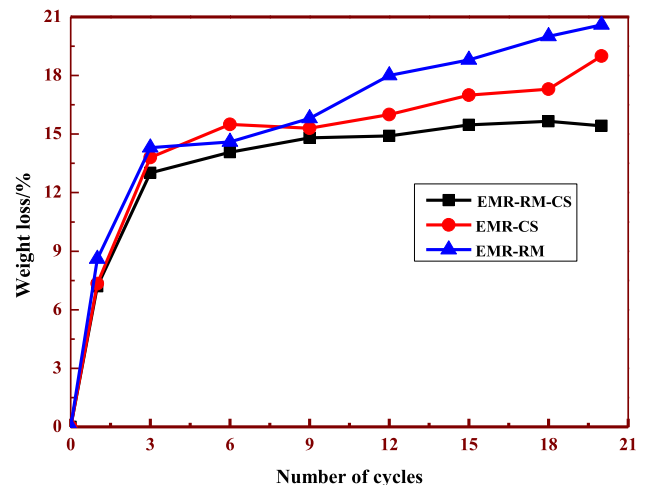


Fig. 7. Mass loss of the road base materials varying with the number of wetting-drying cycles.

As shown in Fig. 6, the UCS of EMR-RM-CS, EMR-CS and EMR-RM after 20 wetting-drying cycles are 6.1 MPa, 1.1 MPa and 1.7 MPa respectively. The strength of EMR-RM-CS still meets the standard of road base material, which implies that it possesses enough wet-dry resistance. However, the strength of the other two groups decreased obviously. It is worth noting that in the EMR-RM-CS and EMR-RM, the UCS of the 1–3 cycles increased gradually. After the third cycle, the strength began to decrease, and the UCS was lower than that of the contrast specimen after the sixth cycle. The main reason is that water immersion promotes hydration reaction at the cycles 1–3, more aluminum participates in the reaction and combines with Ca and Si to produce strength-advantageous products, after 3 cycles, the hydration reaction is terminated, the hydration products no longer increase and the strength begins to decrease; and drying at 70 °C can also accelerate hydration reaction. The combination of hydration reaction and structural transformation is beneficial to the increase of strength. The strength of EMR-CS decreases gradually, mainly due to the fact that the hydration reaction was completed after curing for 28 days, and the hydration reaction could not continue to take place as there was no more Al in the system to form the hydration products. It can be seen from Fig. 7 that the mass loss of different specimens increases with the increase of cycles, and the 1–3 cycles have a larger mass loss, mainly due to the surface mass loss at the initial stage of the cycles, and then the weight loss increased slowly.

The durability test further proves the feasibility of the application of EMR-RM-CS road base material. In order to further observe the strength forming mechanism and structural characterization, the internal structure and hydration products were further analyzed.

### 3.3. MIP analysis

MIP analysis can be able to correlate strength and porosity and microstructure and porosity [33]. Through the analysis of pore structure by MIP method, the total pore volume, average pore size, porosity and pore size distribution can be obtained and then the influence of internal structure on mechanical properties can be inferred [34]. The detailed analysis results of the pore structure are shown in Table 4. The total pore volume decreases under the synergy of EMR-RM-CS. Meanwhile, the average pore diameter and porosity are lowest in EMR-RM-CS, and then has the best pore structure [35]. Bulk density and apparent density were also displayed in Table 4. The higher density corresponds to higher strength because of the higher density of hydration products [36]. It is clear that EMR-RM-CS showed the highest bulk density, and then the density of C-A-S-H gel and AFt are highest, so the highest UCS and durability are exhibited in EMR-RM-CS.

Fig. 8 gives the cumulative porosity and Log-differential volume curve plots of EMR-CS, EMR-RM and EMR-RM-CS based road base material cured for 7 days. The critical pore diameter ( $p_c$ ) and threshold pore diameter ( $p_t$ ) are shifted to smaller pore diameter from EMR-RM to EMR-RM-CS on the Log differential and cumulative porosity plot, respectively.  $p_c$  is based on the peak value of the Log differential curve and  $p_t$  is acquired from the slope of the

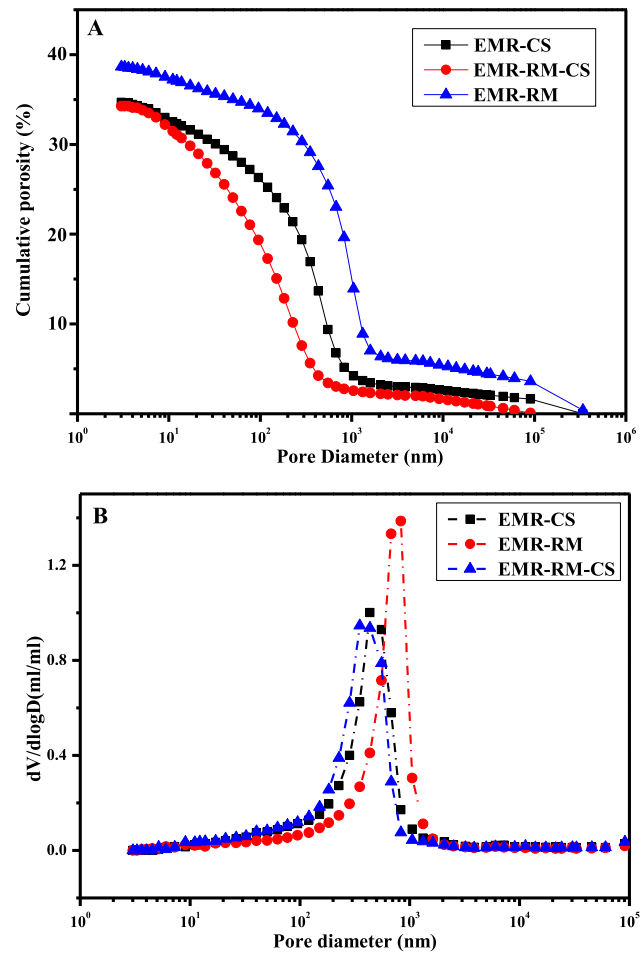


Fig. 8. Cumulative porosity (A) and Log-differential volume (B) curve plots at 7 days for road base material.

cumulative porosity curve [37]. As shown in Fig. 8, the EMR-CS, EMR-RM and EMR-RM-CS show only one peak, the corresponding  $p_c$  value is 0.532  $\mu$ m, 0.918  $\mu$ m and 0.376  $\mu$ m, respectively. However, the pore diameter changed a little. As  $p_c$  means the most frequently occurring pore size in the whole sample [38], which provides extended information on pore structure evolution. It is generally accepted that the smaller the critical pore diameter, the finer the pore structure [39]. So, under the synergistic effect, the EMR-RM-CS based road base material own the lower transmissivity. Also, according to the strength-porosity relationships, higher cumulative porosity slope at the same pore diameter corresponds to higher strength [40], as shown in Fig. 8 that EMR-RM-CS shows the best cumulative porosity, therefore, own higher compressive strength and durability.

### 3.4. XRD analysis

The XRD patterns of EMR-CS, EMR-RM and EMR-RM-CS hydrated for 7 days are presented in Fig. 9. It can be observed from Fig. 9 that the main hydration products are AFt and C-A-S-H gel, which can promote the development of strength. The left phases, like SiO<sub>2</sub>, Fe<sub>2</sub>O<sub>3</sub>, CaCO<sub>3</sub> as well as CaSO<sub>4</sub>·2H<sub>2</sub>O, can be obtained from raw materials. It is worth noting that the new peak of C-A-S-H gel in 8 and 28° only exist in EMR-RM-CS. Also, the amount of hydration products in EMR-RM-CS are highest, and make the internal bonding of road base materials more closely, which is corresponding to the results of UCS and durability.

Table 4  
Pore structure of the hardened pastes hydrated for 7 days.

Sample	Total Pore Volume (mg/L)	Average Pore Diameter (nm)	Porosity (%)	Bulk Density (g/cm <sup>3</sup> )	Apparent/Skeletal Density (g/cm <sup>3</sup> )
EMR-RM	0.4854	94.8	38.42	1.11	2.41
EMR-RM-CS	0.3477	41.6	33.73	1.53	2.38
EMR-CS	0.3926	56.3	35.48	1.39	2.07

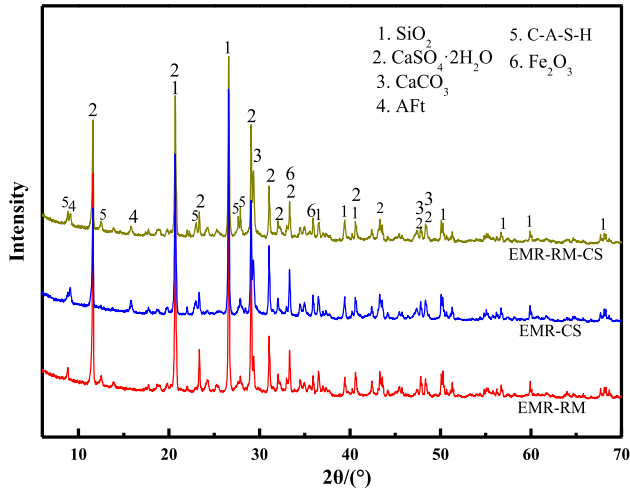
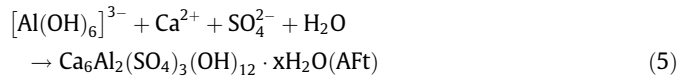
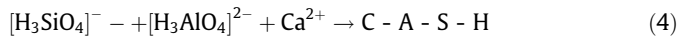
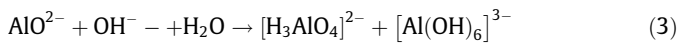
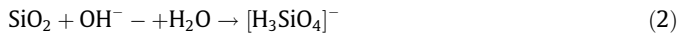


Fig. 9. XRD patterns of the three different road base material curing for 7 days.

The main reason is that RM can provide Al and OH<sup>-</sup>, and EMR has enough CaSO<sub>4</sub>·2H<sub>2</sub>O, which will leach Ca<sup>2+</sup> and SO<sub>4</sub><sup>2-</sup>, CS can provide enough Ca<sup>2+</sup> and OH<sup>-</sup>. When the alkalinity is high, the activity of alumina in red mud will be stimulated. The Al-O and Si-O chemical bond is destroyed by OH<sup>-</sup>, free Al and Si will combine with Ca<sup>2+</sup> and SO<sub>4</sub><sup>2-</sup> to form C-A-S-H gel and AFt. The main reactions are as follows:



Therefore, the strength mechanism of EMR-CS-RM is due to the effectively activated of alkaline and sulfate, more hydraulic substance is formed (C-A-S-H gel and AFt) to provide higher strength. Due to the OH<sup>-</sup> in EMR-RM and Al in EMR-CS are low content, cause hydration reaction incompletely. Low content of C-A-S-H gel and AFt leads to decrease in strength and durability.

### 3.5. <sup>27</sup>Al and <sup>29</sup>Si NMR analysis

<sup>29</sup>Si and <sup>27</sup>Al NMR are characterization tool for both the amorphous and poorly crystalline phases of Si and Al in hardened pastes [41]. <sup>29</sup>Si NMR provides information on the relative amount of silicon atoms in different Q<sup>n</sup> (mAl) (n = 0–4) tetrahedra environments where n is the number of bridge oxygen between [SiO<sub>4</sub>] tetrahedra, and m is the number of Al atoms around the [SiO<sub>4</sub>] tetrahedra [33]. The polymerization degree of the aluminum-silicate chains can be obtained from the <sup>29</sup>Si NMR spectra. Similarly, <sup>27</sup>Al NMR spectra have been used to analyze the coordination of Al [42]. Therefore, the formula for calculating the relative bridge oxygen (RBO) number is summarized [43], which can effectively evaluate the degree of [SiO<sub>4</sub>] polymerization:

$$\begin{aligned} \text{RBO} &= \frac{1}{4} \left( 1 \times \frac{Q^1}{\sum Q^n} + 2 \times \frac{Q^2}{\sum Q^n} + 3 \times \frac{Q^3}{\sum Q^n} + 4 \times \frac{Q^4}{\sum Q^n} \right) \\ &= \frac{1}{4} \frac{\sum n \cdot Q^n}{\sum Q^n} \end{aligned} \quad (6)$$

Q<sup>n</sup>: The relative area of the formant

According to the research of Puertas et al [34], the peaks at –77 ppm to –82 ppm corresponds to Q<sup>1</sup> units; the peaks appearing near –85 to –89 ppm to Q<sup>2</sup> units, the substitution of Si by Al cause the signals to 3–5 ppm to more positive values. So, the peaks around –82 to –84 ppm is to Q<sup>2</sup>(1Al)/Q<sup>2</sup>(0Al); the chemical shift from –92 ppm to –100 ppm is the resonance peak of Q<sup>3</sup> units, therefore, the peak near –88 ppm to –91 ppm is to Q<sup>3</sup>(2Al)/Q<sup>3</sup>(1Al). Previous experiments have shown that in the raw materials, the main peaks are Q<sup>0</sup>, Q<sup>1</sup> and Q<sup>2</sup>, respectively. The <sup>29</sup>Si NMR spectra of EMR-CS, EMR-RM and EMR-RM-CS hydrated pastes cured for 7 days are shown in Fig. 10, the cumulative intensity (I (Q<sup>n</sup>)) and RBO are shown in Table 5. It reveals that the chemical shifts of main resonance peaks are –82.79 ppm, –86.01 ppm, –88.17 ppm, –90.37 ppm and –92.68 ppm, respectively. Which

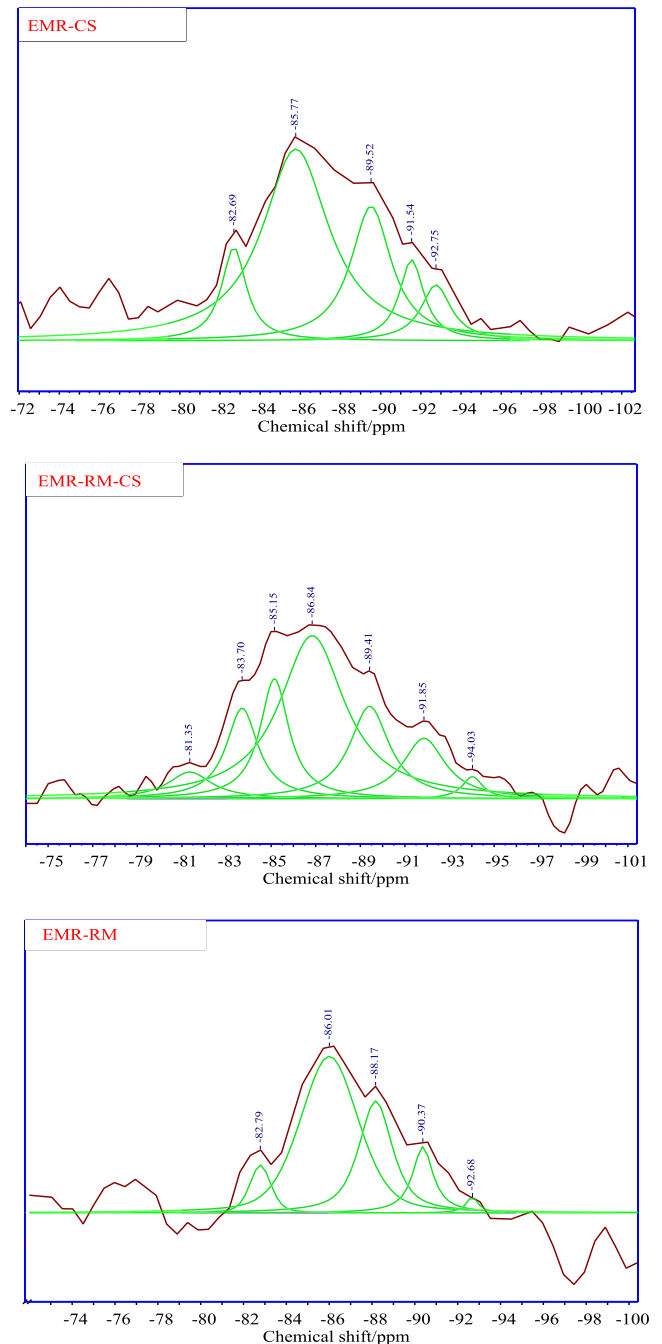


Fig. 10. <sup>29</sup>Si NMR spectra of the three hydrated pastes cured for 7 days.

**Table 5**  
The I(Q<sup>n</sup>) and RBO of the three hydrated pastes cured for 7 days.

Sample	Chemical shift(ppm)	Assign	Relative area	I(Q <sup>n</sup> )	RBO
EMR-RM	-82.79	Q <sup>2</sup> (1Al)	22.73	0.15	59.95%
	-86.01	Q <sup>2</sup>	100.00	1.0	
	-88.17	Q <sup>3</sup> (2Al)	47.35	0.86	
	-90.37	Q <sup>3</sup> (1Al)	31.54	0.29	
	-92.68	Q <sup>3</sup>	2.31	0.02	
EMR-RM-CS	-81.35	Q <sup>1</sup>	13.93	0.19	62.60%
	-83.70	Q <sup>2</sup> (1Al)	40.72	0.57	
	-85.15	Q <sup>2</sup> (0Al)	53.33	0.70	
	-86.84	Q <sup>2</sup>	100	1.00	
	-89.41	Q <sup>3</sup> (2Al)	45.69	0.73	
	-91.85	Q <sup>3</sup> (1Al)	36.50	0.38	
	-94.03	Q <sup>3</sup>	5.17	0.07	
EMR-CS	-82.69	Q <sup>2</sup> (1Al)	25.50	0.38	59.24%
	-85.77	Q <sup>2</sup>	100	1.00	
	-89.52	Q <sup>3</sup> (2Al)	40.45	0.84	
	-91.54	Q <sup>3</sup> (1Al)	14.85	0.30	
	-92.75	Q <sup>3</sup>	18.32	0.23	

represents Q<sup>2</sup>(1Al), Q<sup>2</sup>, Q<sup>3</sup>(2Al), Q<sup>3</sup>(1Al) and Q<sup>3</sup>, respectively. It can be seen that the tetrahedron Si-O in EMR-RM is mainly Q<sup>2</sup> and Q<sup>3</sup>(2Al) units, which has a higher relative area and cumulative intensity. So, the two units are associated with the main hydration products of the road base material. In EMR-CS, the structure of tetrahedron Si-O are the same with EMR-RM, only the chemical shifts of each formant have changed slightly. Obviously, the relative area and cumulative intensity of Q<sup>3</sup> in EMR-CS increased a lot compared to that of EMR-RM, which can explain that the strength and durability of EMR-CS are better than that EMR-RM. In EMR-RM-CS hydrated pastes, the chemical shifts corresponding to the resonance peaks are -81.35 ppm, -83.70 ppm, -85.15 ppm, -86.84 ppm, -89.41 ppm, -91.85 ppm and -94.03 ppm respectively. Compared with EMR-CS and EMR-RM, Q<sup>1</sup> and Q<sup>2</sup>(0Al) appear, resulting in the increase of the confusion degree. Meanwhile, the cumulative intensity of Q<sup>2</sup>(1Al), Q<sup>3</sup>(2Al) and Q<sup>3</sup>(1Al) increased, which caused the amount of [AlO<sub>4</sub>] combined with [SiO<sub>4</sub>] to increase.

From Table 5, it can be seen that the RBO of EMR-RM, EMR-RM-CS and EMR-CS are 59.95%, 62.60% and 59.24% respectively. It indicates that the degree of polymerization of the [SiO<sub>4</sub>] tetrahedra is best in EMR-RM-CS. Under the synergy of the three materials, the quantity of bridge oxygen in tetrahedron Si-O increased; the number of tetrahedrons Al-O replacing tetrahedrons Si-O also increased, and the degree of polymerization of the system increased [43], which was reflected in the higher strength and durability of EMR-RM-CS.

<sup>27</sup>Al NMR spectra from EMR-CS, EMR-RM and EMR-RM-CS hydrated pastes are shown in Fig. 11. As it can be seen that all the three pastes have two strong and sharp peaks around 59.6 ppm and 68 ppm, which are associated to four coordinated aluminum (Al<sup>IV</sup>), and the sharp peak at 60 ppm mainly derived from unreacted four-coordinated aluminum in raw materials [44,45]. The four coordinated aluminum peaks around 68 ppm are due to the interaction of the raw materials [41]. After activation reaction, the four-coordination aluminum was activated and overlapped with the four-resonance aluminum peak in the C-A-S-H gel. Another two smaller peaks near 12 ppm and 4 ppm are six-coordinated aluminum (Al<sup>VI</sup>) [45,46]. The narrow center band at 12 ppm is from the octahedral aluminum structure in Aft, the broad peak at 4 ppm is the inactivated Al<sup>VI</sup> from raw materials.

The relative integral area and relative content of each peak are calculated by Mestrenova. The results are shown in Table 6. It can be observed from Table 6 that the content of activated Al<sup>VI</sup> in EMR-CS, EMR-RM and EMR-RM-CS are 16.48%, 16.47% and 26.94%,

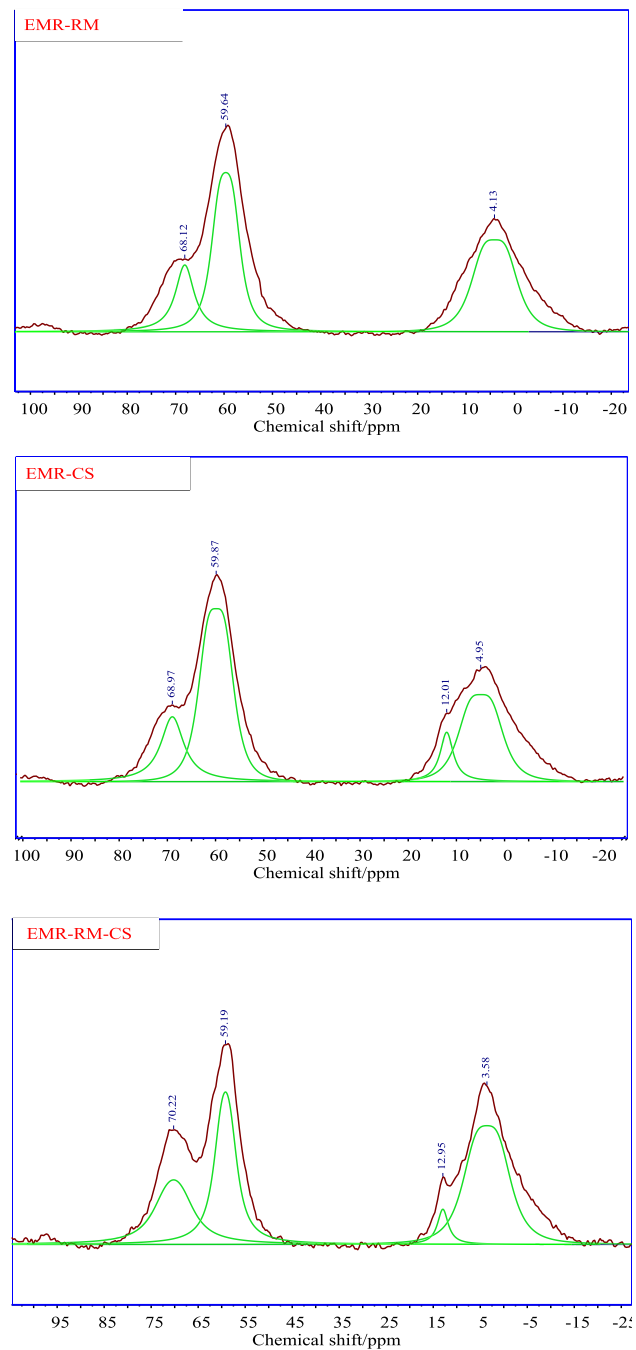


**Fig. 11.** <sup>27</sup>Al NMR spectra of the three hydrated pastes curing for 7 days.

respectively. So, the activated Al<sup>VI</sup> is highest in EMR-RM-CS, and the Al<sup>IV</sup> in EMR-CS, EMR-RM nearly the same. In EMR-RM-CS, the content of stimulated Al<sup>IV</sup> is high, which exist in the chemical shift at 70.22 ppm, the intensity and area of the peak increase obviously. It is clear that the center peak at 12 ppm, which characterizes Al<sup>VI</sup> did not appear in EMR-RM, because there is not sufficient Ca<sup>2+</sup> to form Aft.

According to <sup>27</sup>Al NMR analysis of EMR-CS, EMR-RM and EMR-RM-CS paste hydrated at 7 days, it reveals that the Al in road base materials exists in Al<sup>IV</sup> and Al<sup>VI</sup> but the Al<sup>IV</sup> is dominant. The most part of tetrahedron Al-O binding with tetrahedron Si-O to form C-A-S-H gel and a small part is converted to octahedron Al<sup>VI</sup>, which cause the activated Al in EMR-RM-CS to be high.

**Table 6**  
Results obtained from deconvolution of  $^{27}\text{Al}$  NMR spectra of the three hydrated pastes.

Sample		$\text{Al}^{\text{IV}}$		$\text{Al}^{\text{VI}}$	
		$\text{Al}_1^{\text{IV}}$	$\text{Al}_2^{\text{IV}}$	$\text{Al}_1^{\text{VI}}$	$\text{Al}_2^{\text{VI}}$
EMR-RM	Chemical shift (ppm)	68.97	59.87	12.01	4.95
	Relative peak area	37.47	100	21.26	68.57
	Relative content (%)	16.48	44.00	9.35	30.16
EMR-CS	Chemical shift (ppm)	68.12	59.64	–	4.13
	Relative peak area	34.78	100	–	76.34
	Relative content (%)	16.47	47.37	–	36.16
EMR-RM-CS	Chemical shift (ppm)	70.22	59.19	12.95	3.58
	Relative peak area	68.68	100	6.44	79.88
	Relative content (%)	26.94	39.21	2.52	31.33

More Si and Al participate in hydration reaction lead to the amount of hydration products (C-A-S-H gel and AFt) increased, which own a positive effect on the strength forming [44]. Meanwhile, the degree of polymerization of the system increases with the increase of activated Al and Si, and a better polymerization degree will promote a better polymerization structure [41]. Compared with EMR-CS and EMR-RM, EMR-RM-CS has the highest polymerization degree and the most hydration products (C-A-S-H gel and AFt), exhibit higher UCS and durability.

### 3.6. SEM-EPMA analysis

The microstructure of EMR-RM, EMR-CS and EMR-CS-RM pastes cured for 7 days is displayed in Fig. 12. It can be seen that fibrous C-A-S-H gel, needle-shaped or rod-shaped AFt and  $\text{CaSO}_4 \cdot 2\text{H}_2\text{O}$  can be observed in the hardened pastes of different materials for 7 days. The AFt microcrystals are used to fill the pores and make the structure more compact [47]. The surface of the unreacted par-

ticles was covered with fibrous C-A-S-H gel, which connects all parts of the material together. The C-A-S-H gel and AFt crystallites of EMR-CS-RM is more intensive and the number of products is largest in EMR-CS-RM, resulting in high strength, which is consistent with XRD results. It is noted that though EMR-CS-RM paste is uneven, there is no obvious pore, porosity is low. In contrast, the pores in EMR-RM and EMR-CS are obviously, resulting in poor pore structure, which agrees with MIP results.

EPMA is an analytical tool used to analyze the abundance and distribution of major and trace elements at a microscale in the road base material [44]. Fig. 13 demonstrates the BSE image and element distribution maps of Ca, Si, Al and S in EMR-RM-CS road base material hydrated for 7 days. It depicts that Ca was widely distributed in the matrix, Si, Al and S uniform distribution throughout the matrix. The average level of Ca, Si, Al and S are 233, 56, 27 and 47 respectively. The distribution of four elements is consistent, corresponding to the AFt and C-A-S-H gel, which play an active role in strength development. This agrees with SEM results.

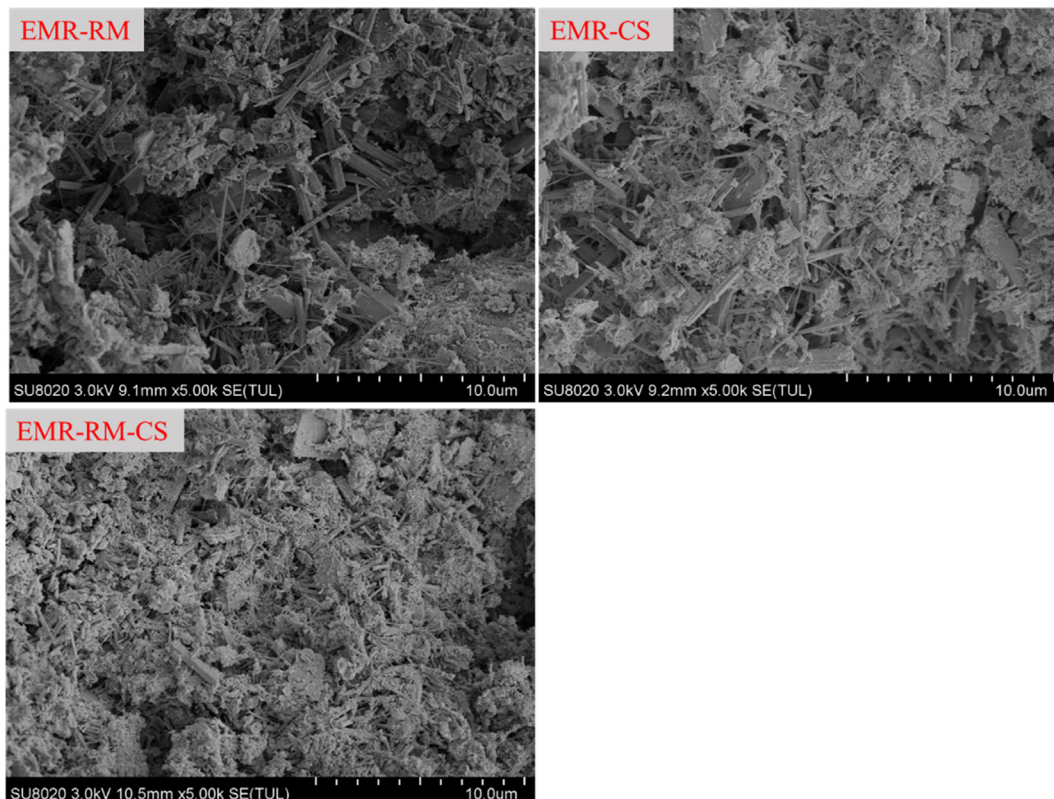


**Fig. 12.** Micrographs of the three hydrated pastes cured for 7 days.

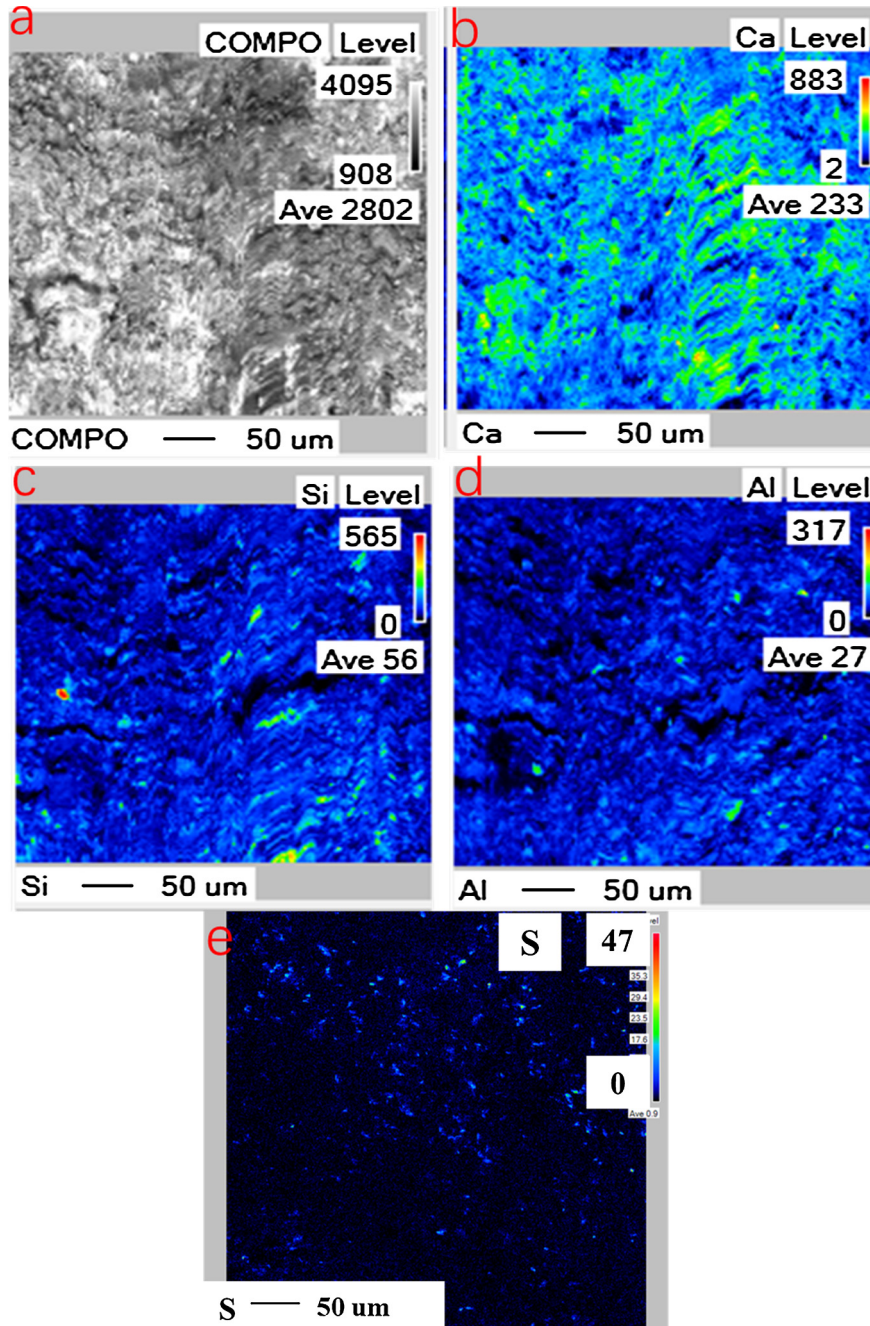


Fig. 13. BSE elemental distribution mapping of Ca, Si, Al and S (b, c, d and e).

### 3.7. Leaching text

Since EMR, RM and CS all contain heavy metal ions, the environmental safety of the road base materials must be considered. The leaching text results of raw materials and the road base materials specimens cured for 7d are listed in Table 7. The acetic acid buffer of pH = 2.64 was used as required by Chinese standards HJ/T 300-2007. The results were compared to groundwater standards GB14848-2017 (I–IV). It can be seen from Table 7 that the main pollutants in EMR are  $Mn^{2+}$  and ammonia nitrogen, while the  $Na^+$  mainly exist in RM. The contents of  $Mn^{2+}$  and  $Na^+$  in raw materials exceed the minimum standard for groundwater GB14848-2017. But the contents of heavy metal ions and ammonia nitrogen in the road base materials synergistically prepared by EMR-CS-RM all meet the standards. Therefore, EMR-CS-RM road base material

has good environmental safety performance, can replace traditional road base materials for road engineering.

Combination with hydration products and previous research theories [44,48], the reason for solidification is that the heavy metals are adsorbed on AFt and C-A-S-H gel matrix. Moreover, Mn can replace Ca to react with Si and Al, and then one part enters the silica-aluminum skeleton and the others are encapsulated or adsorbed by hydration products. Thus, the solidification of heavy metals can be well realized.

### 3.8. Synergistic strength forming mechanism

According to the above Micro-characterization, it can be seen that under the synergistic action of EMR, RM and CS, the increase of strength and durability is mainly due to the amount of hydration

**Table 7**  
Leaching test results.

Content (mg/L)	pH	Mn <sup>2+</sup>	NH <sub>3</sub> -N <sub>2</sub>	Na <sup>+</sup>	Total Cr	Se	Cd <sup>2+</sup>	Pb <sup>2+</sup>
GB/T 14848-2017	Class I 6.5–8.5	Class I 0.05	Class IV 1.5	Class I 100	Class III 0.05	Class I 0.01	Class I 0.0001	Class I 0.005
EMR	6.86	1267	27.44	N. D	0.147	0.769	0.056	0.363
RM	10.91	N. D	N. D	1183.4	0.3041	N. D	0.0044	0.0222
CS	11.10	N. D	N. D	N. D	0.033	N. D	0.02	N. D
Road base material	8.44	0.0013	1.06	56.38	0.014	N. D	0.0001	0.0016

products increased and the change of silicon-aluminum structure in the system: (1) The activity of alumina in red mud will be stimulated and the chemical bond of Al-O and Si-O were broken by OH<sup>-</sup>, the free Al and Si combined with SO<sub>4</sub><sup>2-</sup> which leached from EMR and Ca<sup>2+</sup> supplemented by CS to form a large number of C-A-S-H gel and AFt, which play a positive role in the development of strength. Meanwhile, with the growth of hydration products, the larger pores will be filled, and promote the improvement of pore structure. (2) The bonding ability between Si and Al is enhanced, more Q<sup>2</sup>(1Al), Q<sup>3</sup>(2Al) and Q<sup>3</sup>(1Al) generation, which makes the degree of polymerization of the system higher and has better polymerization structure. Al in road base materials exists in Al<sup>IV</sup> and Al<sup>VI</sup> but the Al<sup>IV</sup> is dominant. The most part of tetrahedron Al-O binding with tetrahedron Si-O to make the silicon-aluminum bonds more tightly connected. The last small part is converted to octahedron Al<sup>VI</sup>, which cause the activated Al in EMR-RM-CS to be high. These are the main reason for the high compressive strength and durability under synergistic action.

### 3.9. Application test

The EMR-RM-CS road base material has been applied in Guizhou, China. The picture of field-test as shown in Fig. 14. The field-test shows that core sampling and texting after curing for

7 days, the performance of the road base is slightly better than the laboratory results, which further illustrates the feasibility of synergistic effect of multi-solid waste to prepare road base material.

## 4. Conclusions

This paper investigated use EMR, CS and RM as the main raw materials to prepare the road base material. After curing for 7 days, the UCS of the mixture reaches 5.6 MPa and it exceeds the strength requirement (3–5 MPa) for highway road base in Chinese standards. The stronger durability, leaching environmental performance and field application better illustrate the feasibility of EMR-RM-CS road base material. Under the synergistic action, the road base material has the best pore structure and polymerized structure, promote the development of strength. More Si and Al participate in the reaction, and the hydration reaction is more sufficient leads to more hydration products (C-A-S-H gel and AFt) produced, which is beneficial for the UCS as well as the solidification of heavy metals. The EMR-RM-CS road base material not only consumes a large quantity of solid waste, protects the ecological environment but also reduce the cost for road base construction as free solid wastes replace expensive natural materials.



**Fig. 14.** Pictures of field-test.

## Declaration of Competing Interest

There is no conflict of interest in this article.

## Acknowledgments

The authors gratefully acknowledge the financial support from the National Natural Science Foundation of China (No. 51574024) and Fundamental Research Funds for the Central Universities (FRF-TP-18-005B1).

## References

- [1] B. Du, C. Zhou, Z. Dan, et al., Preparation and characteristics of steam-autoclaved bricks produced from electrolytic manganese solid waste, *Constr. Build. Mater.* 50 (2014) 291–299.
- [2] Z. Zhu, Review and prospect of China's electrolytic manganese industry in 2018, *China's Manganese Ind.* 36 (01) (2018) 1–5.
- [3] N. Duan, Z. Dan, F. Wang, et al., Electrolytic manganese metal industry experience-based China's new model for cleaner production promotion, *J. Cleaner Prod.* 19 (17–18) (2011) 2082–2087.
- [4] X. Zhu, W. Li, X. Guan, An active dealcalization of red mud with roasting and water leaching, *J. Hazard. Mater.* 286 (2015) 85–91.
- [5] W. Liu, X. Chen, W. Li, et al., Environmental assessment, management and utilization of red mud in China, *J. Cleaner Prod.* 84 (2014) 606–610.
- [6] P. Zhang, R. Lin, J. Yan, Study on red mud glass ceramics, *Nonferrous Met.* 4 (2000) 76–79.
- [7] C. Huang, Y. Deng, X. Xing, et al., Comprehensive utilization of carbide slag, *Jiaozuo Inst. Tech. (Nat Sci)* 23 (2) (2004) 143–146.
- [8] Y. Zhang, C. Kang, X. Li, et al., The treatment and reutilization of carbide slag, *Polyvinyl Chloride* 1 (2001) 52–54 (in Chinese).
- [9] Laia Miró, M.E. Navarro, P. Suresh, et al., Experimental characterization of a solid industrial by-product as material for high temperature sensible thermal energy storage (TES), *Appl. Energy* 113 (2014) 1261–1268.
- [10] V.K. Sharma, F. Fortuna, M. Mincarini, et al., Disposal of waste types for energy recovery and safe environment, *Energy Convers. Manage.* 65 (1) (1998) 381–394.
- [11] Q. Li, Q. Liu, B. Peng, et al., Self-cleaning performance of TiO<sub>2</sub> – coating cement materials prepared based on solidification/stabilization of electrolytic manganese residue, *Constr. Build. Mater.* 106 (2016) 236–242.
- [12] R. Zhao, L. Han, Preparation of geopolymer using electrolytic manganese residue, *Key Eng. Mater.* 591 (2014) 130–133.
- [13] P.E. Tsakiridis, S. Agatzini-Leonardou, P. Oustadakis, Red mud addition in the raw meal for the production of Portland cement clinker, *J. Hazard. Mater.* 116 (1) (2004) 103–110.
- [14] X. Liu, B. Tang, H. Yin, Durability and environmental performance of Bayer red mud-coal gangue-based road base material, *J. Beijing Univ. Sci. Technol.* 4 (2018).
- [15] N. Zhang, H. Sun, X. Liu, et al., Early-age characteristics of red mud-coal gangue cementitious material, *J. Hazard. Mater.* 167 (1–3) (2009) 927–932.
- [16] Y. Li, R. Sun, C. Liu, etc., CO<sub>2</sub> capture by carbide slag from chlor-alkali plant in calcination/carbonation cycles, *Int. J. Greenhouse Gas Control* 9 (none) (2012) 117–123.
- [17] J. Cao, F. Liu, Q. Lin, et al., Hydrothermal synthesis of xonotlite from carbide slag, *Prog. Nat. Sci.: Mater. Int.* 18 (9) (2008) 1147–1153.
- [18] Y. Liu, W. Ni, X. Huang, Characteristics of hydration and hardening of red mud of Bayer process in carbide slag-flue gas desulfurization gypsum system, *Mater. Rep.* 30 (14) (2016) 120–124.
- [19] P. Chen, K. Liang, Y. Zhao, et al., Study on activation of steel slag by red mud and electrolytic manganese slag composite[J], *Concrete* 10 (2018) 67–73.
- [20] American Society for Testing and Materials, ASTM D698-78, Moisture Density Relations for Soils and Soil-Aggregate Mixtures.
- [21] American Society for Testing and Materials, ASTM D1883, California Bearing Ratio (CBR) of Laboratory-Compacted Soils.
- [22] American Society for Testing and Materials, ASTM D2850-87, Standard Test Method for Unconsolidated, Undrained Compressive Strength of Cohesive Soils in Triaxial Compression.
- [23] S. Kim, A. Hanif, I. Jang, Incorporating Liquid Crystal Display (LCD) Glass Waste as Supplementary Cementing Material (SCM) in Cement Mortars-Rationale Based on Hydration, Durability, and Pore Characteristics, *Materials* 11 (12) (2018) 2538.
- [24] C. Hu, H. Ma, Statistical analysis of backscattered electron image of hydrated cement paste, *Adv. Cem. Res.* 28 (7) (2016) 469–474.
- [25] C. Hu, Z. Li, A review on the mechanical properties of cement-based materials measured by nanoindentation, *Constr. Build. Mater.* 90 (2015) 80–90.
- [26] C. Hu, Z. Li, Property investigation of individual phases in cementitious composites containing silica fume and fly ash, *Cem. Concr. Compos.* 57 (2015) 17–26.
- [27] C. Hu, Multi-scale Characterization of Concrete Ph.D. Thesis, Hong Kong University of Science and Technology, Hong Kong, China, 2014.
- [28] Y. Kim, A. Hanif, M. Usman, et al., Influence of bonded mortar of recycled concrete aggregates on interfacial characteristics – Porosity assessment based on pore segmentation from backscattered electron image analysis, *Constr. Build. Mater.* 212 (2019) 149–163.
- [29] S. Horpibulsuk, M. Hoy, P. Witchayaphong, et al., Recycled asphalt pavement-fly ash geopolymer as a sustainable stabilized pavement material, *Mater. Sci. Eng. Conf. Ser.* (2017) 012005.
- [30] GB/T 50123-1999. Standard for soil test method. Ministry of Construction, P. R. China (in Chinese).
- [31] S.B. Salah, S. Hossain, M. Faysal, et al., Effect of Wet-Dry Cycle on Durability of Cement-Stabilized Recycled Pavement Base Aggregates, in: International Congress and Exhibition " Sustainable Civil Infrastructures: Innovative Infrastructure Geotechnology", Springer, Cham, 2017, pp. 98–114.
- [32] M. Hoy, R. Rachan, S. Horpibulsuk, et al., Effect of wetting-drying cycles on compressive strength and microstructure of recycled asphalt pavement-Fly ash geopolymer, *Constr. Build. Mater.* 144 (2017) 624–634.
- [33] X. Chen, G. Zhu, M. Zhou, et al., Effect of organic polymers on the properties of slag-based geopolymers, *Constr. Build. Mater.* 167 (2018) 216–224.
- [34] L. Cui, J.H. Cahyadi, Permeability and pore structure of OPC paste, *Cem. Concr. Res.* 31 (2) (2001) 277–282.
- [35] J. Zhou, G. Ye, K.V. Breugel, Characterization of pore structure in cement-based materials using pressurization-depressurization cycling mercury intrusion porosimetry (PDC-MIP), *Cem. Concr. Res.* 40 (7) (2010) 1120–1128.
- [36] A. Hanif, P. Parthasarathy, H. Ma, et al., Properties improvement of fly ash cenosphere modified cement pastes using nano silica, *Cem. Concr. Compos.* 81 (2017) 35–48.
- [37] Hongyan Ma, Mercury intrusion porosimetry in concrete technology: tips in measurement, pore structure parameter acquisition and application, *J. Porous Mater.* 21 (2) (2014) 207–215.
- [38] K.K. Aligzaki, Pore Structure of Cement-based Materials: Testing, Interpretation and Requirements, Taylor and Francis, London and New York, 2006.
- [39] Ana Fernández-Jiménez, F. Puertas, I. Sobrados, et al., Structure of calcium silicate hydrates formed in alkaline-activated slag: influence of the type of alkaline activator, *J. Am. Ceram. Soc.* 86 (8) (2004) 1389–1394.
- [40] X. Chen, S. Wu, J. Zhou, Influence of porosity on compressive and tensile strength of cement mortar, *Constr. Build. Mater.* 40 (2013) 869–874.
- [41] X. Liu, N. Zhang, Y. Yao, etc. Micro-structural characterization of the hydration products of bauxite-calcination-method red mud-coal gangue based cementitious materials, *J. Hazard. Mater.* 262 (2013) 428–438.
- [42] F. Puertas, A. FernándezJiménez, M.T. Blancovarela, Pore solution in alkali-activated slag cement pastes. Relation to the composition and structure of calcium silicate hydrate, *Cem. Concr. Res.* 34 (1) (2004) 139–148.
- [43] M.D. Andersen, H.J. Jakobsen, Jørgen Skibsted, Incorporation of Aluminum in the Calcium Silicate Hydrate (C–S–H) of Hydrated Portland Cements: A High-Field <sup>27</sup>Al and <sup>29</sup>Si MAS NMR Investigation, *Inorg. Chem.* 42 (7) (2003) 2280–2287.
- [44] X. Liu, X. Zhao, H. Yin, et al., Intermediate-calcium based cementitious materials prepared by MSWI fly ash and other solid wastes: hydration characteristics and heavy metals solidification behavior, *J. Hazard. Mater.* 349 (2018) 262–271.
- [45] N. Zhang, X. Liu, H. Sun, et al., Pozzolanic behavior of compound-activated red mud-coal gangue mixture, *Cem. Concr. Res.* 41 (3) (2011) 270–278.
- [46] E. Lippmaa, A. Samoson, M. Magi, High-resolution aluminum-27 NMR of aluminosilicates, *J. Am. Chem. Soc.* 108 (8) (1986) 1730–1735.
- [47] N. Zhang, H. Sun, X. Liu, et al., Early-age characteristics of red mud-coal gangue cementitious material, *J. Hazard. Mater.* 167 (1–3) (2009) 927–932.
- [48] D. Peng, G. Wang, X. Liu, et al., Preparation, characterization, and application of an eco-friendly sand-fixing material largely utilizing coal-based solid waste, *J. Hazard. Mater.* 373 (2019) 294–302.